AUTOMATIKA
2021, VOL. 62, NO. 3–4, 503–512
https://doi.org/10.1080/00051144.2021.1989891

Motion synchronization for the SHA/EMA hybrid actuation system by using an optimization algorithm

Waheed Ur Rehman [a], Xinhua Wang[a], Yiqi Cheng[a], Hui Chai[a], Zeeshan Hameed[b], Xingjian Wang[c], Farrukh Saleem[d] and Ehtisham Lodhi[e]

[a]College of Mechanical Engineering and Applied Electronics Technologies, Beijing University of Technology, Beijing, People's Republic of China; [b]School of Microelectronics Chongqing University, Chongqing, People's Republic of China; [c]School of Automation Science and Electrical Engineering, Beihang University, Beijing, People's Republic of China; [d]Department of Modern Mechanics, School of Engineering, University of Science and Technology, Hefei, People's Republic of China; [e]Institute of Automation, Chinese Academy of Sciences, Beijing, People's Republic of China

ABSTRACT

The current research develops a mathematical model and control strategies to address two major problems force fighting and precise position tracking for a hybrid actuation system composed of servo-hydraulic actuator and electro-mechanical actuator (SHA/EMA). The force fighting and desired position tracking are two essential problems of the SHA/EMA actuation system for a large civil aircraft. The trajectory-based fractional order proportional integral derivative (FOPID) control for the SHA/EMA actuation system is proposed, tuned with the help of the particle swarm optimization (PSO) technique and implemented with the support of the FOMCON toolbox in Matlab. The experiments are performed under different external aerodynamic loads that the aircraft usually experiences during flight operations. The results show that the proposed method shows better results for tracking performance, force fighting and load rejection ability.

ARTICLE HISTORY
Received 10 March 2020
Accepted 30 August 2021

KEYWORDS
Servo hydraulic actuator; electromechanical actuator; FOPID control; PID control; motion synchronization

1. Introduction

In more electric aircraft (MEA), we try to reduce the hydraulic components and replace them with electrical components. It has helped to reduce the cost and weight of aircraft [1]. Airbus A380 is an example of large commercial aircraft that was released in 2007. There are two hydraulic and two electrical power networks (2H/2E) in Airbus A380. The two electric network (2E) uses 8 EHA for rudders and spoilers and 8 EBHA for ailerons and elevators. The two hydraulic (2H) network uses 29 SHA. In Boeing 787, five electromechanical actuators (EMA) are involved, four EMA are used for spoilers and one EMA is used for trim horizontal stabilizer (THS). The redundant actuation systems are introduced into the flight control system to increase the reliability of the actuation system. The redundant actuation system may be similar or dissimilar. There are two standard dissimilar redundant configurations, SHA/EHA and SHA/EMA, which are used in more electric aircraft to increase the reliability of the aircraft actuation system. SHA/EMA are preferred over SHA/EHA because SHA and EMA are different in dynamics. If a failure of SHA occurs due to environmental variables, then it is not necessary that EMA will also fail due to the same environmental conditions because both SHA and EMA are different in dynamics [2,3].

The actuation part is a significant element in an aeroplane, which operates a control surface to handle the aeroplane's behaviour and flight track [4]. Mainly, hydraulic power is used to drive the actuation system of aircraft for a long time. The progress and advancement in the aircraft industry have demanded introducing a similar redundant hydraulic actuation system to increase the safety and reliability in the aircraft. However, in the case of a common-mode/common-cause error, it would be a safety risk if we have a hybrid actuation system that consists of two similar redundant actuators. A similar redundant actuation system is not so good for safety and reliability [3]. To introduce an electro-mechanical actuator (EMA) in the hybrid actuation system (HAS) would be more beneficial in a primary flight control [5,6].

Consequently, the hybrid actuation configuration, composed of two different actuators, electro-mechanical actuators (EMA) and electro-hydraulic servo actuators (SHA), is measured as an enhancement in safety and reliability for modern aeroplane design [7]. The research towards more electric aircraft allows us to develop electrical distribution systems, electric motors, actuators, generator drives, and highly reliable power electronics to enhance the performance and reduce the cost [8,9]. Therefore, the hybrid actuation system SHA/EMA, composed of an EMA and an SHA can meet the demand for safety and reliability because this hybrid configuration would efficiently eliminate the common-mode/common-cause errors and introduce

CONTACT Waheed Ur Rehman wrehman87@gmail.com

the robustness and enhance the aeroplane actuation system's efficiency [10]. The hybrid actuation system (HAS) has force-fighting issues that needto be fixed. Different dynamic responses are observed for the same input signal because the EMA and SHA have different working principles. Static force equalization is achieved by adding offsets in position control loop while dynamic force equalization is achieved by forcing hybrid system to follow same tracking path [11]. When different actuators are combined like a hybrid configuration to manoeuvre the control surface over a rigid coupling, there would be an intercoupling effect between the outputs of EMA and SHA. Whenever the control surface is driven by these two different actuators, all the above-mentioned issues arise in the form of a force-fighting issue. This force-fighting issue not only affects the accuracy of tracking control but also damages the control surface. Consequently, we need to develop a controller for HAS to resolve the problem of non-synchronous outputs from two dissimilar actuators, which is a significant problem in the current aviation industry [11,12]. The precision and tracking accuracy can be increased by considering the external disturbances nonlinear dynamics, and the coupling effect in the hybrid actuation system.

Several authors tried their best to solve the problem of force fighting and position tracking for the redundant actuation system (the hybrid actuation system). For example, in [13,14], an intelligent controller is designed using fuzzy logic to address the problem of force fighting and position tracking for the HA/EHA system. Adaptive control techniques, such as the MIT rule and model reference control, are employed to synchronize the motion between HA and EHA [15,16]. [17–19] tried to force (compel) the HA/EHA system to follow trajectory motion state's signals (position, velocity and acceleration signals) for motion synchronization. Various control techniques, such as integral sliding mode control, LPV- and LPV-based integral sliding mode control, are used to solve the problem of the force fighting with precise motion tracking for the HA/EHA system [20–23]. An integral action controller that is designed uses position and force signals to reduce force fighting. Position signal reduces force fighting more efficiently than force signal [24]. A PID control is used to solve the problem of force fighting [25]. Feed-forward control also helps match the dynamics of both actuators [26]. Cochoy's et al. have used displacement, velocity and force signals to reduce force fighting between actuators [5]. An author presented an adaptive decoupling controller that eliminates coupling terms to reduce force fighting and improve position tracking performance for the HA/EHA actuation system [26]. But still, the research is open in this field, and the challenging task is to improve the tracking performance with minimum force fighting.

Most the research work focuses on the SHA/EHA actuation system, while the current research work will focus on the SHA/EMA actuation system. The current research work presents a (third-order) trajectory-based motion synchronization control for the SHA/EMA actuation system using a fractional-order controller. The fractional-order PID controller (FOPID) is tuned using optimization algorithms, such as particle swarm optimization (PSO). The motivation for using FOPID is that it has a wide range of stability areas compared to the PID controller. Furthermore, the FOPID controller has more tuning parameters than the PID controller. The results are compared with published literature (method of Cochoy et al [5]) to verify the effectiveness of the present study. The main paper contents are modelling of the SHA/EMA system, controller design through machine learning techniques, and then the results and discussion part are followed by conclusions.

2. Problem formulation

The principal parts of the SHA/EMA hybrid actuation system are shown in Figure 1. There are two control signals u_{sv} and u_m. u_{sv} is responsible for controlling the position of SHA, while u_m is responsible for controlling the position of EMA. The SHA and EMA are coupled to keep in motion the aircraft's control surface. SHA is a servo valve-based position control actuation system, and EMA is an electric motor-based position control actuation system.

Force fighting issue: When both actuators drive together with the aircraft's control surface, then it creates a force fighting problem. Force fighting shows force difference between two actuators. The mathematical representation of force fighting is given by

$$\gamma = F_s - F_m \tag{1}$$

$$\gamma = k_s x_s - k_m x_m \tag{2}$$

where γ is the force fighting, and it must be zero to make sure both actuators are equal contributing to driving the control surface. The reason behind force fighting is that the electric motor's response time is large significant compared to the servo valve in SHA. The long duration of response time in EMA makes it slower as compared to SHA. Furthermore, the gear mechanism and ball screw make EMA slower than. Equations (1) and (2) show that there will be no force fighting if displacements of both actuators synchronize with each other.

3. Mathematical model of the SHA/EMA system

The hybrid actuation system consists of three main components: SHA, EMA and Control surface. Let them model one by one.

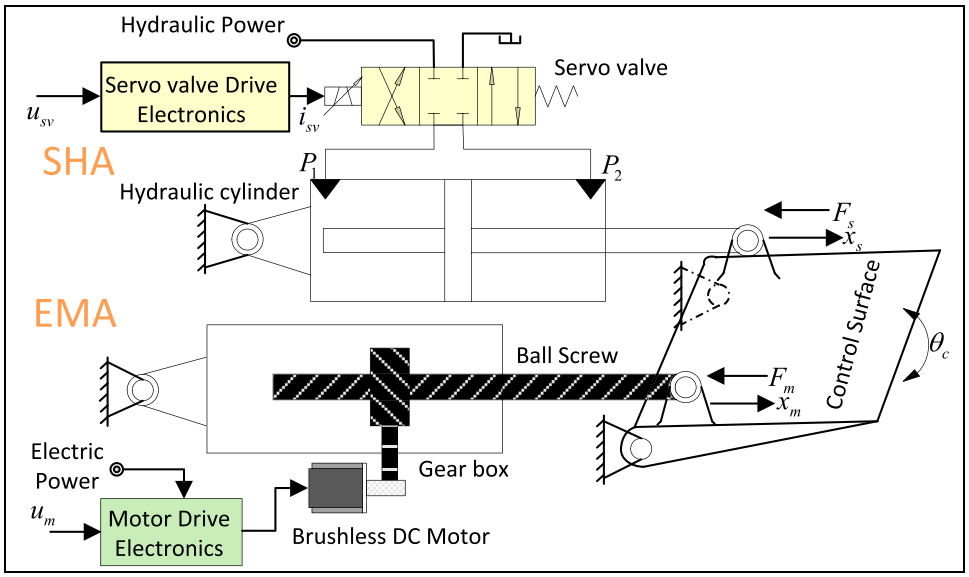

Figure 1. The structure of the SHA/EMA actuation system.

3.1. Mathematical model of the aircraft control surface

The dynamics of the control surface, shown in Figure 1, is given by

$$(F_s + F_m)r_c = j_c\ddot{\theta}_c + F_{air}r_c \tag{3}$$

$$F_s = k_s(x_s - x_c) \tag{4}$$

$$F_m = k_m(x_m - x_c) \tag{5}$$

where r_c is the radial distance for the aircraft control surface, j_c is the moment of inertia of the control surface, θ_c is the rotational displacement of the control surface and F_{air} is the disturbance created by air on the control surface. k_s and k_m are transmission stiffnesses of SHA and EMA, respectively. Normally, the value of angular displacement is very small in such cases θ_c and x_c are taken to be linear [27] and can be described by the following relationship,

$$x_c = \theta_c r_c \tag{6}$$

3.2. Mathematical model of SHA

The opening of a servo valve is a function of input command signal and supply pressure, and this relationship is given by

$$x_{sv} = f(p_s, u_{sv}) \tag{7}$$

where x_{sv} is the servo valve displacement, u_{sv} is the input voltage to the servo valve and p_s is the supplied pressure. The influence of supply is neglected. So, the relation between input voltage and displacement is given by [15]

$$\tau_{sv}\dot{x}_{sv} = k_{sv}u_{sv} - x_{sv} \tag{8}$$

Fluid power is controlled and modulated by the hydraulic servo valve. The flow through the valve is given by

$$Q_{sv} = k_{sq}x_{sv}\sqrt{\left|1 - \frac{p_f}{p_s - p_r}\mathrm{sgn}(x_{sv})\right|} \times \left(1 - \frac{p_f}{p_s - p_r}\mathrm{sgn}(x_{sv})\right) - k_{sc}p_f \tag{9}$$

Flow is linear near null opening and null load points [28], leading to the following form of the flow.

$$Q_{sv} = k_{sq}x_{sv} - k_{sc}p_f \tag{10}$$

where k_{sq} is the flow/opening gain before null pressure drop, k_{sc} is the flow/pressure gain and p_f is the load pressure.

The flow, which is given to the hydraulic jack by the servo valve, is consumed in rod velocity, leakage and hydraulic compression. So, the flow for chamber 1 Q_{j1} and chamber 2 Q_{j2} is given by

$$\begin{cases} Q_{j1} = A_j\dot{x}_s + \dfrac{v_1 + A_j x_s}{E_j}\dot{p}_1 + k_{ac}p_f \\ Q_{j2} = A_j\dot{x}_s - \dfrac{v_2 - A_j x_s}{E_j}\dot{p}_2 + k_{ac}p_f \end{cases} \tag{11}$$

where k_{ac} is the leakage coefficient for jack and E_j is the bulk modulus of oil in hydraulic jack. The chamber volume v_1 and v_2 are taken to be identical and assumed to be half of the total jack's volume. The flow delivered to the jack is given by

$$Q_{sv} = \frac{Q_{j1} + Q_{j2}}{2} = A_j\dot{x}_s + \frac{v_j}{4E_j}\dot{p}_f + k_{ac}p_f \tag{12}$$

where A_j is the effective area of the piston of the jack and v_j is an effective volume of the jack's chamber. There is a pressure difference between two chambers of hydraulic

jack which creates a hydraulic jack force which is consumed to produce dynamic motion characteristics of the rod of the jack. It is given by

$$\begin{aligned} F_j &= m_j\ddot{x}_s + B_j\dot{x}_s + F_s \\ F_j &= A_j p_f \end{aligned} \tag{13}$$

where F_j is the force produced by the hydraulic jack, m_j is the mass of the piston of jack, B_j is the damping constant of the hydraulic jack.

Define $x_1 = [x_{11}, x_{12}, x_{13}, x_{14}]^T = [x_s, \dot{x}_s, \ddot{x}_s, \dddot{x}_s]^T$ as the state vector of the SHA system. Suppose that $k_{ce} = k_{ac} + k_{sc}$, and $u_1 = u_{sv}$. Then, the state space form of SHA can be described by

$$\Omega_{SHA} = \begin{cases} \dot{x}_{11} = x_{12} \\ \dot{x}_{12} = x_{13} \\ \dot{x}_{13} = x_{14} \\ \dot{x}_{14} = f_1(x_1) + g_1 + \sigma_1 u_1 \end{cases} \tag{14}$$

where

$$\begin{aligned} f_1(x_1) &= -ax_{14} - bx_{13} - cx_{12} - dx_{11} \\ a &= \left(\frac{4E_jA_j}{V_jm_j\tau_{sv}}\right)\left(\frac{V_jB_j\tau_{sv}}{4E_jA_j} + \frac{V_jm_j}{4E_jA_j} + \frac{\tau_{sv}k_{ce}m_j}{A_j}\right) \\ b &= \left(\frac{4E_jA_j}{V_jm_j\tau_{sv}}\right)\left(\tau_{sv}A_j + \frac{V_jB_j}{4E_jA_j} + \frac{\tau_{sv}k_{ce}B_j}{A_j} + \frac{k_{ce}B_j}{A_j} + \frac{k_sV_j\tau_{sv}}{4E_jA_j}\right) \\ c &= \left(\frac{4E_jA_j}{V_jm_j\tau_{sv}}\right)\left(A_j + \frac{k_{ce}B_j}{A_j} + \frac{k_sk_{ce}\tau_{sv}}{A_j} + \frac{k_sV_j}{4E_jA_j}\right) \\ d &= \left(\frac{4E_jA_j}{V_jm_j\tau_{sv}}\right)\left(\frac{k_sk_{ce}}{A_j}\right)g_1 = \left(\frac{4E_jA_j}{V_jm_j\tau_{sv}}\right) \\ &\quad \times \left[\frac{k_sV_j\tau_{sv}}{4E_jA_j}\ddot{x}_c + \left\{\frac{k_sk_{ce}\tau_{sv}}{A_j} + \frac{k_sV_j}{4E_jA_j}\right\}\dot{x}_c \right. \\ &\quad \left. + \frac{k_sk_{ce}}{A_j}x_c\right]\sigma_1 = \frac{4E_jA_jk_{sq}k_{sv}}{m_jv_j\tau_{sv}} \end{aligned}$$

3.3. Mathematical model of EMA

The EMA actuator shown in Figure 1, has the following integral parts: a ball screw (actuation mechanism), gear box and brushless DC motor [27]. The electrical dynamics of the brushless DC motor is based on Newton's 2nd law and Kirchhoff's voltage law. These dynamics are described by the following relationship.

$$u_m = k_m\omega_m + L_m\frac{di_m}{dt} + R_mi_m \tag{15}$$

where i_m is the armature current of the motor, R_m is the armature resistance, L_m is the armature inductance of motor, ω_m is the angular velocity of motor's rotator. The torque, generated by the DC motor, has a proportional relationship with the armature's current and magnetic field strength. The magnetic field is constant here, so it is assumed that the torque is directly proportional to the current of the armature coil by a constant factor. This is often referred to as armature controlled motor. The torque dynamics of the motor is given by

$$T_m = k_{bm}i_m \tag{16}$$

where k_{bm} is the back emf constant and T_m is the electromagnetic torque. It has been shown that the motor provides torque due to the input signal to its armature coils. This torque produced mechanical dynamics. This torque is transferred to the mechanical structure (gear mechanism, ball screw mechanism and connected shafts). This torque is converted into inertial motion, which overcomes damping dynamics and load torque dynamics. The mechanical dynamics are given by

$$\begin{aligned} T_m - T_L &= j_m\frac{d\omega_m}{dt} + T_f \\ T_f &= B_m\omega_m \end{aligned} \tag{17}$$

where B_m is the damping coefficient of the electromechanical actuator, j_m is the total moment of inertia for all rotating parts and T_L is the loaded torque. The transition relation between translational and rotation parts is described as

$$\begin{cases} \dot{x}_m = \dfrac{1}{\eta_m k_{gm}}\omega_m \\ T_L = \dfrac{1}{\eta_m k_{gm}}F_m \end{cases} \tag{18}$$

where η_m and k_{gm} are transmission efficiency and transmission coefficient of gear and ball screw mechanism in the EMA actuation system, respectively.

Define $x_2 = [x_{21}, x_{22}, x_{23}]^T = [x_m, \dot{x}_m, \ddot{x}_m]^T$ as the state vector of the EMA system and suppose $u_2 = u_m$. The state-space form of EMA is described as

$$\Omega_{EMA} = \begin{cases} \dot{x}_{21} = x_{22} \\ \dot{x}_{22} = x_{23} \\ \dot{x}_{23} = f_2(x_2) + g_2 + \sigma_2 u_2 \end{cases} \tag{19}$$

where $f_2(x_2) = -\frac{R_mk_{ms}}{L_mj_mk_{gm}^2\eta_m^2}x_{21} - \frac{k_{bm}k_mk_{gm}^2\eta_m^2 + L_mk_{ms} + R_mB_mk_{gm}^2\eta_m^2}{L_mj_mk_{gm}^2\eta_m^2}x_{22} - \frac{B_mL_m + j_mR_m}{j_mL_m}x_{23}g_2 = \frac{R_mk_{ms}}{L_mj_mk_{gm}^2\eta_m^2}x_c + \frac{k_{ms}}{j_mk_{gm}^2\eta_m^2}\dot{x}_c$, $\sigma_2 = \frac{k_{bm}}{L_mj_mk_{gm}\eta_m}$

4. The proposed design strategy

The proposed design strategy has two FOPID controllers. The FOPID controller generates an output signal for SHA and EMA. The FOPID controller takes its input signal from a trajectory. Particle swarm optimization (PSO) is used to obtain the parameters of the FOPID controller using a multi-variable objective function. Furthermore, theFOPID controller takes

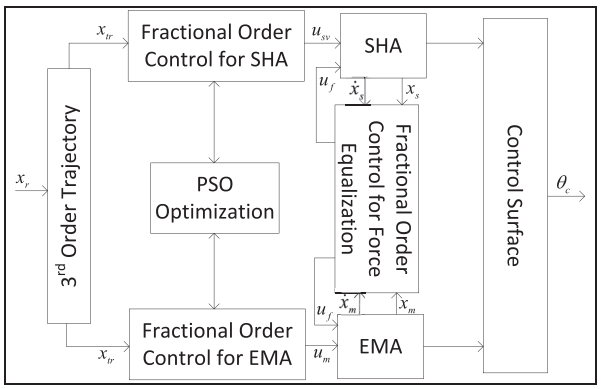

Figure 2. Schematic diagram of controller implementation.

the position and velocity signal of two actuators and generates an output signal that helps for synchronization motion of two actuators. Both actuators drive the control surface with an angular displacement of θ_c. The schematic diagram of controller implementation is shown in Figure 2.

4.1. Trajectory

The desired dynamics are generated by the trajectory, which takes the reference signal as input and generates position, velocity and acceleration signal as output. The current research will use a third-order trajectory. The motivation for using the third-order trajectory is that the SHA is at least a fifth-order and EMA is at least a fourth-order, so a third-order trajectory performs better for the SHA/EMA actuation system. Furthermore, a third-order trajectory is also advantageous due to its three design parameters $(\tau_i, \xi_i, \omega_i)$. These design parameters are chosen in such a way that force fighting is minimized. The canonical form of third-order trajectory, used by the SHA/EMA system, is given by

$$G = \frac{1}{(\tau_i s + 1)\left(\frac{1}{\omega_i^2}s^2 + \frac{2\xi_i}{\omega_i}s + 1\right)} \tag{20}$$

4.2. FOPID control

The FOPID controller, a type of PID controller, was introduced by Podlubny [29]. The control law in T-domain and S-domain for such a controller is defined as

$$\begin{aligned} u(t) &= k_p e(t) + k_i I_t^{-\lambda} e(t) + k_d D_t^{-\mu} e(t) \\ C(s) &= k_p + k_i s^{-\lambda} e(t) + k_d s^{-\mu} \\ &\therefore \{k_p, k_i, k_d, \lambda, \mu\} \in R \end{aligned} \tag{21}$$

where $I_t^{-\lambda}$ and $D_t^{-\mu}$ are the integral and derivative fractional operators, respectively. λ and μ are the integral and derivative fractional powers, respectively. The k_d, k_i, k_p are derivative, integral and proportional gains, respectively.

4.3. Multi-objective performance criteria

There were several criteria for tuning controller parameters, such as ISE, IAE and ITSE which represent integral of square error, absolute error or time square error. The present research will use the multi-objective performance criteria to tune the parameters of the FOPID controller. The multi-objective performance criteria used by the current research are given by

$$\begin{aligned} f(k) = w_1 &\left[\sum_0^t (x_{tr} - x_h)^2 + \sum_0^t (x_{tr} - x_m)^2\right] \\ &+ w_2 \sum_0^t (F_s - F_m)^2 + w_3[|T_s|] \\ &+ w_4[|T_r|] + w_5[|O_s|] \end{aligned} \tag{22}$$

where $k \in [k_p, k_i, k_d, \lambda, \mu]$, w_1, w_2, w_3, w_4, w_5 are weighted gains. Increasing the gain value for specific gain results in improving performance criteria of that term and degrade in performance criteria of other terms. The value for weighted gains is given by

$$w_1 = 1, w_2 = 1 \times 10^{-11}$$
$$w_3 = \frac{1}{7}, w_4 = 1, w_5 = \frac{1}{9}$$

4.4. Particle swarm optimization (PSO)

The optimization algorithms for tuning parameters of controllers are getting popular these days [30–34]. A 10-dimensional vector is introduced to adjust the parameters of FOPID for SHA and EMA by using particle swarm optimization. This 10-dimensional vector is given by

$$(k_{ph}, k_{ih}, k_{dh}, \lambda_h, \mu_h, k_{pm}, k_{im}, k_{dm}, \lambda_m, \mu_m)$$

There are some terms for particle swarm optimization that are very important to describe before describing the steps for particle swarm optimization.

(1) Θ is a fundamental element of PSO whose value is given by

$$\Theta = [\theta_1, \theta_2, \theta_3, \theta_4, \theta_5, \theta_6, \theta_7, \theta_8, \theta_9, \theta_{10}]$$
$$\Theta = [k_{ph}, k_{ih}, k_{dh}, \lambda_h, \mu_h, k_{pm}, k_{im}, k_{dm}, \lambda_m, \mu_m]$$

Θ gives us a solution for tuning parameters of the FOPID controller. The ith particle for nth iteration is given by

$$\Theta_i(n) = [\theta_{i,1}(n), \theta_{i,2}(n), \theta_{3,i}(n) \ldots \theta_{10,i}(n)]$$

There are upper and lower bounds $[\theta_{\min}, \theta_{\max}]$on the optimizing tuning parameters.

$$\theta_j = \begin{cases} \theta_{\min} & \text{if } \theta_j < \theta_{\min} \\ \theta_j & \text{if } \theta_{\min} \le \theta_j \le \theta_{\max} \\ \theta_{\max} & \text{if } \theta_j > \theta_{\max} \end{cases} \tag{23}$$

(2) Velocity $V(n)$: represents the particle's moving velocity $\Theta(n)$. The ith particle's velocity for nth iteration is given by

$$V_i(n) = [v_{i,1}(n), v_{i,2}(n), v_{i,3}(n) \ldots v_{i,10}(n)] \quad (24)$$

(3) Individual best $P(n)$ is obtained by comparing the current cost function value with the best cost function value. The particle that has the best cost function value is called individual best. The individual best for the ith particle is obtained by obeying the following condition

$$J(P_i(n)) \leq J(\Theta_i(\tau)) \therefore \tau \leq n \quad (25)$$

where $J(\Theta_i)$ and $J(P_i)$ are the cost functions for Θ_i and P_i, respectively. The ith individual best is given by

$$P_i(n) = [p_{i,1}(n), p_{i,2}(n), p_{i,3}(n) \ldots p_{i,10}(n)] \quad (26)$$

(4) The global best value: it is the best value among individual best values. The global best value is given by

$$G(n) = [g_1(n), g_2(n), g_3(n), \ldots, g_{10}(n)] \quad (27)$$

The global best value is obtained in such a way that it holds the following conditions.

$$J(G(n)) \leq J(P_i(n)) \backslash i = 1, 2, \ldots, H \quad (28)$$

(5) Velocity and Position: These are updated according to the global best value and individual values. The mathematical representation for velocity and position of a particle is given by

$$\begin{aligned} v_{i,j}(n+1) &= w v_{i,j}(n) + c_1 r_1 (p_{i,j}(n) - \theta_{i,j}(n)) \\ &\quad + c_2 r_2 (g_j(n) - \theta_{i,j}(n)) \backslash i = 1, 2, 3 \ldots, H \\ \theta_{i,j}(n+1) &= \theta_{i,j}(n) + v_{i,j}(n+1) \quad \backslash j = 1, 2, 3, \ldots \end{aligned} \quad (29)$$

where $v_{i,j}(n)$ is a current velocity and $v_{i,j}(n+1)$ is the next velocity, r_1 and r_2 are two random numbers, w is the inertial weight, c_1 and c_2 are positive acceleration constants.

(6) Termination criteria: There are two types of termination conditions. The first one is to obtain the desired number of iterations, while the second one is to obtain the desired values of objective or cost function. The current research will choose the first condition to perform optimization for the required number of iterations.

All design steps, to tune the parameters of the FOPID controller for SHA and EMA, are as follows.

Step 1: A multi-variable objective function is defined. This objective function is calculated by performing simulations in Simulink and updating the variables, such as settling time, rise time, percentage overshoot, force fighting and error signal into Matlab workspace for each iteration. The parameters, such as w, c_1 and c_2 and required number iterations, are defined.

Step 2: Stop PSO if the required number of iterations has been obtained; else, update the objective function by performing simulations for the next iteration.

Step 3: Find the individual best to hold the condition of Equation (25).

Step 4: Find the value of global best to hold the condition of Equation (28).

Step 5: Update the position and velocity of particles by Equation (29). Apply the upper and lower bounds with the help of Equation (23).

Step 6: Go to step 2.

5. Result and discussion

To check the performance of the proposed method, the simulation experiments are performed in Matlab/Simulink by using simulation parameters given in Table 1. The results are compared with those of Cochoy's method. The tracking performances of the proposed method and Cochoy's method [5] are compared in Table 2**,** while the force-fighting analysis is given in Table 3.

5.1. Simulation results with a square impulse load

A pilot command of 30 mrad is given to the SHA/EMA hybrid actuation system at 0.1 s with an external force of

Table 1. Parameters for the SHA/EMA actuation system [7,11,14].

	Parameters	Values
(SHA)	Servo valve gain k_{sv}	3.04×10^{-4} m/A
	Flow/opening gain k_{sq}	2.7 m^2/s
	Flow/pressure gain k_{sc}	1.75×10^{-11} (m^3/s)Pa
	Piston area of SHA A_j	1.1×10^{-3} m^2
	Cylinder chamber volume v_j	1.1×10^{-4} m^3
	Mass of piston and chamber m_j	25 kg
	Damping coefficient B_j	1×10^4 Ns/m
	Bulk modulus E_j	8×10^8 Pa
	Leakage coefficient k_{ac}	1×10^{-11} (m^3/s)Pa
(EMA)	Back Induced emf constant k_m	0.161 V/(rad/s)
	Motor's armature inductance L_m	4.13×10^{-3} H
	Motors' armature resistance R_m	0.54 Ω
	Electromagnetic coefficient k_{bm}	0.64 Nm/A
	Total inertia of rotating parts j_m	1.136×10^{-3} kg m^2
	Damping coefficient B_m	4×10^{-3} Nm.s/rad
	Transmission coefficient k_{gm}	1.256×10^3 rad/m
	Transmission efficiency η_m	0.9
Control Surface	Connection stiffness of SHA k_s	1×10^8 N/m
	Connection stiffness of EMA k_m	1×10^8 N/m
	Radial distance r_{cs}	0.1 m
	Moment of inertia j_{cs}	6.0 kg m^2

Table 2. Tracking performance.

	Performance parameters (s)			Maximum tracking error under load (mm)		
Control Techniques	Rise time	Settling time	Overshoot	Square impulse load	Sinusoidal wave load	Real-time wave loads
Cochoy's Method	0.4231	1.3019	2.7450	5	7.1	5
Proposed Method	0.2893	0.5734	0.8978	3	4.1	3

Table 3. Force-fighting comparisons.

Control Techniques	Maximum force fighting in magnitude (N)			
	Without load	Square impulse load	Sinusoidal wave load	Real-time wave loads
Cochoy's Method	7000	6500	4600	6440
Proposed Method	500	1900	2500	1565

15KN. The external disturbance (load) force is a square impulse load that acts at 1.5 s. The square impulse load works for 3 s with an impulse of 50% duration. The maximum initial force fighting for Cochoy's method is 7000 N when there is no load, while the maximum force fighting for Cochoy's method is 6500 N when external force acts on it. The external force comes in the form of impulse disturbance for 3 s. The maximum initial force fighting for the present method is 500 N when there is no load, while the maximum force fighting for the present method is 1900 N when external force acts on it. The present method shows better results than Cochoy's method concerning force fighting. It can be seen from Table 3 that the present method has less force fighting than Cochoy's method under the same conditions. Cochoy's method has 7000 N force fighting, while the present method has 500 N under no-load, which shows better performance of the proposed method. Similarly, Cochoy's method has 6500 N force fighting, while the present method has 1900 N under impulse load disturbance. This shows better performance of the proposed technique or method. Force-fighting results are shown in Figure 3. The tracking performance is the second most important factor for comparison. A pilot command is a step input signal of 30 mrad.

Figures 4 and 5 show that the SHA/EMA hybrid actuation system follows the desired pilot command signal more efficiently under the proposed method rather than under Cochoy's method. The maximum tracking error is 5 mrad when the SHA/EMA actuation system is controlled by Cochoy's method, while it is 3 mrad when the SHA/EMA actuation system is controlled by the proposed method. It shows that tracking

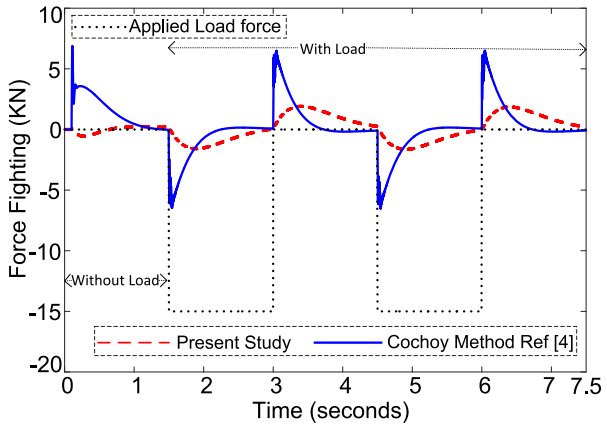

Figure 3. Comparison of force fighting.

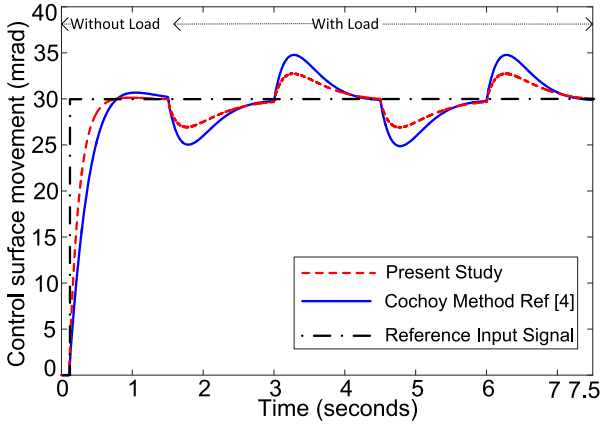

Figure 4. Comparison of tracking performance.

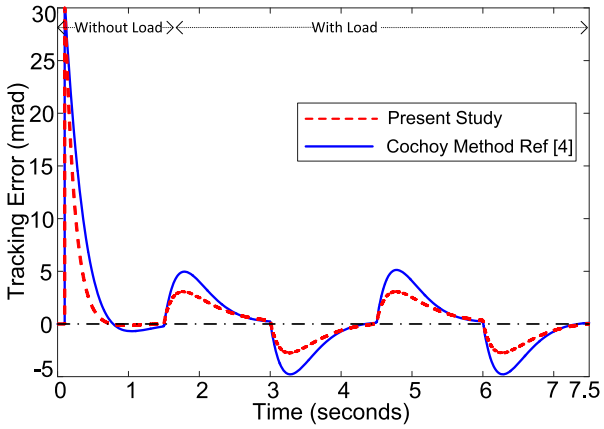

Figure 5. Comparison of tracking error.

error is less when the system is controlled by the proposed method than Cochoy' method. A comparison between tracking performance under different control strategies is shown in Table 2**.**

5.2. Simulation results with a sinusoidal wave load

A pilot command of 30 mrad is given to the SHA/EMA hybrid actuation system at 0.1 s with an external force of 15 KN amplitude. The external disturbance (load) force is a sinusoidal wave load that acts at 1.5 s. The sinusoidal wave load acts with a frequency π rad/s. Cochoy's method for the SHA/EMA actuation, system under sinusoidal wave load, has 4600 N force fighting. In contrast, force fighting reduces to 2500N when the same SHA/EMA actuation system is operated by the present method. It clearly shows that the SHA/EMA actuation system controlled by the present method shows better performance for force fighting. A comparison of the force fighting between Cochoy's method and the present technique is shown in Table 3 and Figure 6.

The hybrid SHA/EMA actuation system, with the help of control strategy, is assumed to follow the desired pilot command signal by facing external load disturbance. The results in Figures 7 and 8 show that SHA/EMA hybrid actuation system follows the desired

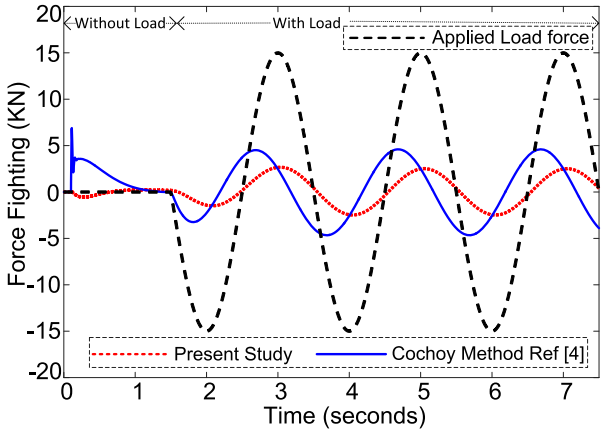

Figure 6. Comparison of force fighting.

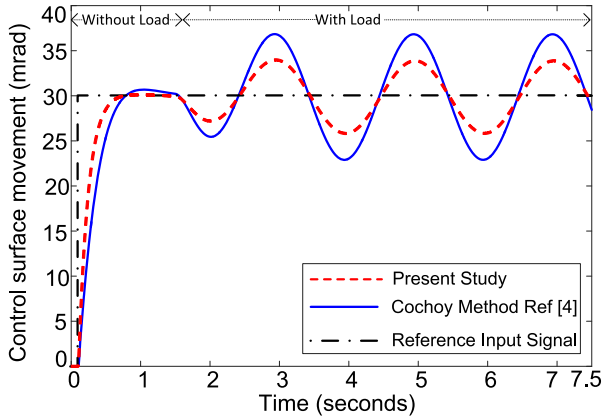

Figure 7. Comparison of tracking performance.

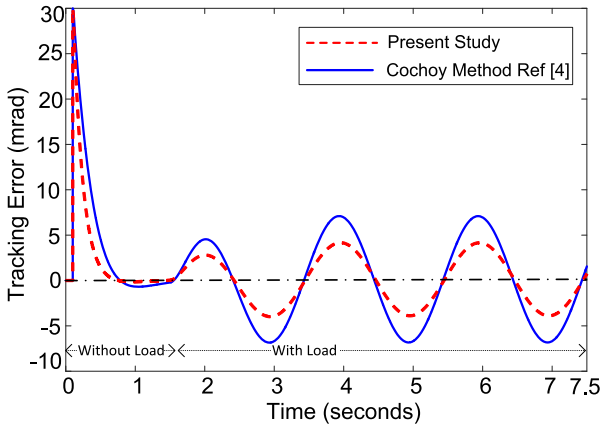

Figure 8. Comparison of tracking error.

pilot command signal more efficiently under the present method rather than under Cochoy's method. When the system is controlled by Cochoy's method, then the maximum tracking error is 7.1 mrad for the SHA/EMA actuation system, while it is 4.1 mrad when the SHA/EMA actuation system is controlled by the present method. It shows that tracking error is less when the system is controlled by the present method as compared to Cochoy's method. A comparison between tracking performance under different control strategies is shown in Table 2.

5.3. Simulation results with a realtime wave load

The real-time flight control system usually faces the external load disturbance with multiple frequencies and amplitudes. To cope with real-time flight control problems, an external load disturbance is created with multiple frequencies and amplitudes. The performance of the SHA/EMA hybrid actuation system under two different control strategies is checked by facing this external load disturbance. The SHA/EMA actuation system controlled by Cochoy's method has 6440N force fighting, while force fighting reduces to 1565N when the same SHA/EMA actuation system is controlled by the present method. It shows that the SHA/EMA actuation system shows better performance under the present method even it is subjected to real-time load signal. A comparison of force fighting between Cochoy's method and the present method is shown in Table 3 and Figure 9.

The hybrid SHA/EMA actuation system, with the help of a control strategy, is assumed to follow the desired pilot command signal by facing external load disturbance. The results in Figures 10 and 11 show that the SHA/EMA hybrid actuation system follows the desired pilot command signal more efficiently under the proposed method rather than under Cochoy's method. The maximum tracking error is 5 mrad for the

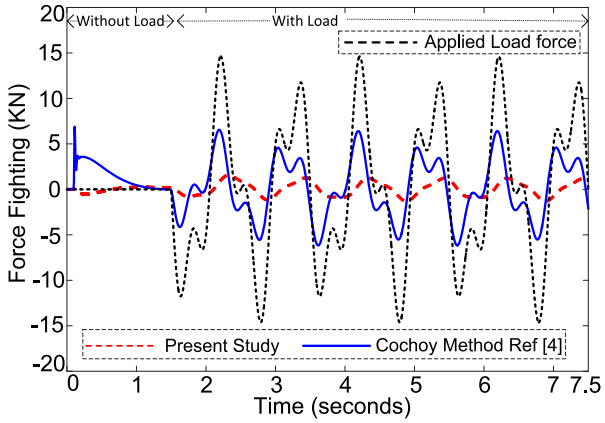

Figure 9. Comparison of force fighting.

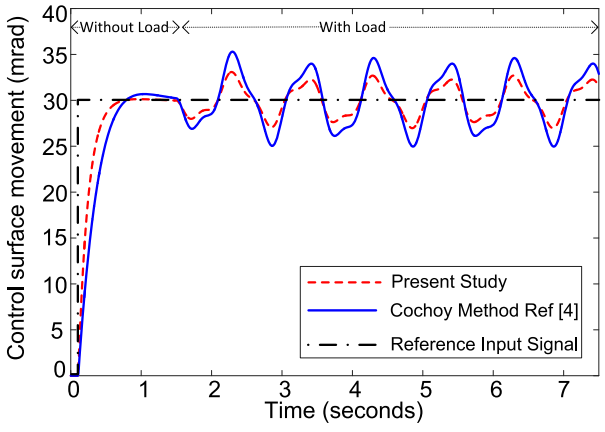

Figure 10. Comparison of tracking performance.

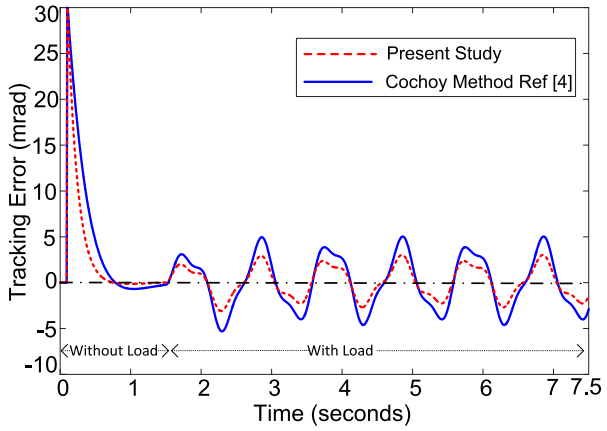

Figure 11. Comparison of tracking error.

SHA/EMA actuation system when the system is controlled by Cochoy's method, while it is 3 mrad when the SHA/EMA actuation system is controlled by the proposed method. It shows that tracking error is less when the system is controlled by the proposed method compared to Cochoy's method. A comparison between tracking performance under different control strategies is shown in Table 2.

6. Conclusions

The research work focuses on reducing force fighting and improving the position tracking performance of the control surface for the SHA/EMA actuation system of a prominent civil aircraft. Force fighting problems occur due to different motion dynamics of SHA and EMA. The research work designs a higher-order trajectory-based fractional-order control system for the SHA/EMA actuation system. The tuning parameters are found using particle swarm optimization with a multi-variable objective function. The objective function considers performance specifications, coupling terms, tracking error and performance characteristics so that we can obtain a better set of tuning parameters. The performance of the proposed technique is checked for the SHA/EMA actuation system under pilot step input command, by facing different types of external load disturbance on the control surface of aircraft. The results show that the proposed technique shows better results for tracking performance, force fighting and load rejection performance. The proposed technique also shows better robust behaviour under different forms of external load disturbance.

Disclosure statement

No potential conflict of interest was reported by the author(s).

Funding

The author is very thankful to Beijing university of Technology and Chinese Government for supporting research work under the following research grants No. 2017YFC0805005-1. The Natural Science and Foundation of China under Project number 51075008.

ORCID

Waheed Ur Rehman http://orcid.org/0000-0002-5649-7381

References

[1] Jones R. The more electric aircraft – assessing the benefits. Proc Inst Mech Eng G: J Aerosp Eng. 2002;216(5):259–269.
[2] Fu J, Fu Y, Zhang P. Status and development of electrically powered actuators for aerospace application. CSAA/IET International Conference on Aircraft Utility Systems (AUS 2018); 2018., pp. 270–275: IET.
[3] Van Den Bossche D. The A380 flight control electrohydrostatic actuators, achievements and lessons learnt. 25th International Congress of the Aeronautical Sciences; 2006., pp. 1–8.
[4] Goupil P. AIRBUS state of the art and practices on FDI and FTC in flight control system. Control Eng Pract. 2011;19(6):524–539.
[5] Cochoy O, Hanke S, Carl UB. Concepts for position and load control for hybrid actuation in primary flight controls. Aerosp Sci Technol. 2007;11(2-3):194–201.
[6] Fu J, Maré J-C, Fu Y. Modelling and simulation of flight control electromechanical actuators with special focus on model architecting, multidisciplinary effects and power flows. Chin J Aeronaut. 2017;30(1):47–65.
[7] Cochoy O, Carl UB, Thielecke F. Integration and control of electromechanical and electrohydraulic actuators in a hybrid primary flight control architecture. International Conference on Recent advances in Aerospace Actuation Systems and Components; 2007. pp. 1–8: INSA Toulouse.
[8] Emadi K, Ehsani M. Aircraft power systems: technology, state of the art, and future trends. IEEE Aerosp Electron Syst Mag. 2000;15(1):28–32.
[9] Naayagi R. A review of more electric aircraft technology. 2013 International Conference on Energy Efficient Technologies for Sustainability; 2013. pp. 750–753: IEEE.
[10] Rosero J, Ortega J, Aldabas E, et al. Moving towards a more electric aircraft. IEEE Aerosp Electron Syst Mag. 2007;22(3):3–9.
[11] Wang L, Mare J-C. A force equalization controller for active/active redundant actuation system involving servo-hydraulic and electro-mechanical technologies. Proc Inst Mech Eng G: J Aerosp Eng. 2014;228(10): 1768–1787.
[12] Qi H, Mare J-C, Fu Y. Force equalization in hybrid actuation systems. 7th International Conference on Fluid Power Transmission and Control, Hangzhou; 2009, pp. 342–347.
[13] Waheed UR, Wang S, Wang X, et al. A position synchronization control for HA/EHA system. 2015 International Conference on Fluid Power and Mechatronics (FPM); 2015, pp. 473–482.
[14] Rehman WU, Wang S, Wang X, et al. Motion synchronization in a dual redundant HA/EHA system by using a hybrid integrated intelligent control design. Chin J Aeronaut. 2016;29(3):789–798.
[15] Rehman WU, Wang S, Wang X, et al. Adaptive control for motion synchronization of HA/EHA system by using modified MIT rule. 2016 IEEE 11th Conference

on Industrial Electronics and Applications (ICIEA); 2016, pp. 2196–2201.
[16] Rehman WU, Wang X, Wang S, et al. Motion synchronization of HA/EHA system for a large civil aircraft by using adaptive control. 2016 IEEE Chinese Guidance, Navigation and Control Conference (CGNCC); 2016, pp. 1486–1491.
[17] Rehman WU. Trajectory based motion synchronization in a dissimilar redundant actuation system for a large civil aircraft). 2017 29th Chinese control and Decision Conference (CCDC); 2017.
[18] Wang X, Shi C, Wang S. Extended state observer-based motion synchronisation control for hybrid actuation system of large civil aircraft. Int J Syst Sci. 2017;48(10):2212–2222.
[19] Wang X, Liao R, Shi C, et al. Linear extended state observer-based motion synchronization control for hybrid actuation system of more electric aircraft. Sensors. 2017;17(11):1–16.
[20] Ijaz S, Yan L, Hamayun MT. Fractional order modeling and control of dissimilar redundant actuating system used in large passenger aircraft. Chin J Aeronaut. 2018;31(5):1141–1152.
[21] Ijaz S, Yan L, Hamayun MT, et al. An adaptive LPV integral sliding mode FTC of dissimilar redundant actuation system for civil aircraft. IEEE Access. 2018;6:65960–65973.
[22] Ijaz S, Hamayun MT, Anwaar H, et al. LPV modeling and tracking control of dissimilar redundant actuation system for civil aircraft. Int J Control Autom Syst. 2019;17(3):705–715.
[23] Ijaz S, Hamayun MT, Yan L, et al. Adaptive fault tolerant control of dissimilar redundant actuation system of civil aircraft based on integral sliding mode control strategy. Trans Inst Meas Control. 2019;41(13):3756–3768.
[24] Fan D, Fu Y, Chen J, et al. An accurate, nonlinear model and control of hybrid actuation system (WIP). In Proceedings of the 2014 Summer Simulation Multiconference, 2014, pp. 1–8.
[25] Zhang Y, Yuan Z. Control strategy of aileron's force-fight. Int J Multimed Ubiquitous Eng. 2014;9(8):299–310.
[26] Shi C, Wang X, Wang S, et al. Adaptive decoupling synchronous control of dissimilar redundant actuation system for large civil aircraft. Aerosp Sci Technol. 2015;47:114–124.
[27] Guo LL, Yu LM, Lu Y, et al. Multi-mode switching control for HSA/EHA hybrid actuation system. Appl Mech Mater. 2014;494:1088–1093.
[28] MARE J-C. Actionneurs hydrauliques. commande. Tech ing, Inform ind. 2002;2(S7531):S7531–1-S7531.
[29] Podlubny I. Fractional-order systems and PI/sup/spl lambda//D/sup/spl mu//-controllers. IEEE Trans Automat Contr. 1999;44(1):208–214.
[30] Jigang H, Hui F, Jie W. A PI controller optimized with modified differential evolution algorithm for speed control of BLDC motor. Automatika. 2019;60(2):135–148.
[31] Sadalla T, Horla D, Giernacki W. Stability region of a simplified multirotor motor–rotor model with time delay and fractional-order PD controller. Automatika. 2017;58(4):384–390.
[32] Sivalingam R, Chinnamuthu S, Dash SS. A modified whale optimization algorithm-based adaptive fuzzy logic PID controller for load frequency control of autonomous power generation systems. Automatika. 2017;58(4):410–421.
[33] Zhang M, Ma Z, Chen L, et al. Missile fixed-structure μ controller design based on constrained PSO algorithm. Automatika. 2017;58(3):312–320.
[34] El Gmili N, Mjahed M, El Kari A, et al. Particle swarm optimization based proportional-derivative parameters for unmanned tilt-rotor flight control and trajectory tracking. Automatika. 2020;61(2):189–206.